INTERNATIONAL JOURNAL FOR NUMERICAL METHODS IN FLUIDS
Int. J. Numer. Meth. Fluids 2006; **50**:1003–1027
Published online 15 November 2005 in Wiley InterScience (www.interscience.wiley.com). DOI: 10.1002/fld.1102

The numerical study of roll-waves in inclined open channels and solitary wave run-up

Yin-Tik Que[‡] and Kun Xu[*,†]

Mathematics Department, Hong Kong University of Science and Technology, Clear Water Bay, Kowloon, Hong Kong

SUMMARY

In this paper, we introduce a finite-volume kinetic BGK scheme and its applications to the study of roll and solitary waves. The current scheme is based on the numerical solution of the gas-kinetic Bhatnagar–Gross–Krook model in the flux evaluation across each cell interface. An intrinsic connection between the BGK model and time-dependent, non-linear, non-homogeneous shallow-water equations enables us to solve shallow-water equations automatically with our kinetic scheme. The analytical solution, experimental measurements, and numerical calculations for problems associated with roll-waves down an inclined open channel and solitary waves incident on a sloped beach are also presented. Copyright © 2005 John Wiley & Sons, Ltd.

KEY WORDS: gas-kinetic scheme; shallow water equations; roll wave; solitary wave

1. INTRODUCTION

Shallow-water equations model free-surface flow of layers of incompressible fluids under the influence of gravity when the vertical dimension is assumed to be much smaller than any typical horizontal scale. In other words, these equations model long wavelength phenomena. They act as the basis of many mathematical models in use for the simulation of certain fluid flow phenomena. Dam-break waves, bore wave propagation, hydraulic jumps, roll-waves in open channel flow, waves breaking on sloping beaches, among others, can be reasonably described by shallow-water equations [1]. The equations are derived from the depth-averaged incompressible Navier–Stokes equations where the hydrostatic pressure distribution is assumed. The resulting equations present a system of non-linear conservation laws of mass and momentum.

*Correspondence to: Kun Xu, Mathematics Department, Hong Kong University of Science and Technology, Clear Water Bay, Kowloon, Hong Kong.
†E-mail: makxu@ust.hk
‡E-mail: csdee@ust.hk

Contract/grant sponsor: Hong Kong Research Grant Council; contract/grant numbers: HKUST6116/03E, HKUST-6102/04E, HIA04/05.EG02

Received 5 May 2005
Revised 3 August 2005
Accepted 11 August 2005

The conservation laws describing the motion of the shallow-water flow are a time-dependent system of non-linear partial differential equations of hyperbolic type, which admit smooth as well as discontinuous solutions. The discontinuity indicates hydraulic jumps or bores when they occur on the surface of hydraulic fluid and is comparable to a shock wave in gas dynamics.

There are many numerical approaches to solving shallow-water equations. The Godunov and kinetic schemes are two of them. Godunov scheme is based on the Riemann solution using the exact or approximate Riemann solver in the gas evolution stage, while the kinetic scheme uses the microscopic particle distribution function as the basis to construct the fluxes. The Boltzmann equation provides a complete and correct treatment of dynamical processes in gas at low density, but its complexity prohibits a transparent characterization of its solutions. Kinetic models have been used to make useful approximations to the Boltzmann equation. Model kinetic equations are obtained by replacing the collision operator in the Boltzmann equation with a simpler, more tractable form that preserves its most important features. One successful kinetic model for the Boltzmann equation, called the BGK model, was developed by Bhatnagar, Gross, and Krook in 1954 [2]. This model ignores details of molecular collisions and replaces the correct collision term by a simpler approximate form. The intrinsic connection between the BGK kinetic model and the non-homogeneous shallow-water equations leads to the result that shallow-water equations are solved automatically from the BGK scheme. The particle velocity change due to gravitational force can be used to recover the non-homogeneous term in the shallow-water equations to simulate the flow motion in a varying bottom topography [3].

The governing equations for the shallow-water theory and kinetic equation are presented in Section 2, and the corresponding finite-volume discretizations are described. For example, Section 2.2 considers the flux evaluation in the BGK scheme with the inclusion of the gravitational force term. Sections 3 and 4 present our application of the BGK kinetic model. The first example focuses on the problem of roll-waves moving down an inclined open channel, in which the shallow-water equations with source terms that model the balance between the slope and the friction of the river bottom must be solved. This problem closely follows the paper by Brook–Falle–Pedley [4]. Some parameter values and variables are not described very clearly in that paper and may lead the reader into uncertainties following the numerical procedure. In the current study, parameter values for the problem are justified again, and the details are made as clear as possible. Linear analysis of the problem of a uniform flow down a sloping channel is considered to establish the stability condition. The evolution of roll-waves emerging out of an initially uniform flow is a result of instability. The roll-waves and the amplitude growth or decay of the flow are simulated from the BGK scheme. The procedure for constructing the analytical roll-wave solution described by Dressler [5] is summarized and the result is compared with the numerical one. Section 4 considers the run-up of a solitary wave incident on a uniform sloping beach connected to an open ocean with constant depth, the so-called tsunamis phenomenon. The numerical result obtained from the BGK scheme is compared with experimental measurements [6].

2. GOVERNING EQUATIONS AND FINITE-VOLUME FORMULATIONS

A commonly used approach for modelling water flows with free surfaces under the influence of gravity is to solve shallow-water equations, which can be obtained from depth averaging

of the Navier–Stokes equations. The derivation of the shallow-water equations is from the approximate shallow water theory, which is based upon the assumption that the vertical component of the acceleration of the water particles has a negligible effect on the pressure. The full derivation can be found in References [1, 7–9]. The theory is so named because it describes flows in which the vertical dimensions are small compared with the horizontal dimensions. The resulting shallow-water equations are time-dependent systems of non-linear, hyperbolic partial differential equations (PDEs) representing conservation of mass and momentum, and the solution may admit discontinuities (e.g. shocks, which are equivalent to bore waves and hydraulic jumps in the shallow-water flow).

One-dimensional shallow-water equations with bottom topography expressed in conservation-law form in a river channel of unit width are given by

$$\begin{aligned} &\frac{\partial h}{\partial t}+\frac{\partial}{\partial x}(hU)=0 \quad \text{(Continuity equation)} \\ &\frac{\partial}{\partial t}(hU)+\frac{\partial}{\partial x}\left(hU^2+\frac{1}{2}Gh^2\right)=-Gh\frac{\mathrm{d}B}{\mathrm{d}x}-C_{\mathrm{f}}U^2 \quad \text{(Momentum equation)} \end{aligned} \tag{1}$$

where t denotes time, x is the distance along the channel, $h(x,t)$ is the water height above the river bottom, $U(x,t)$ is the water velocity averaged across the water height in the x-direction, and G is the acceleration due to gravity, given by the constant value, $G=9.8\,\mathrm{m\,s^{-2}}$. $B=B(x)$ is the bottom elevation along the river channel, so the surface level, $\eta(x,t)$, is given by $h(x,t)+B(x)$. A sketch of a river channel with bottom topography in one dimension is depicted in Figure 1. The bed slope term, $-GhB'(x)$, accounts for the dynamical effect on the fluid motion from the gravitational force and the varying river bottom. The friction force between the water and the river bottom is modelled by $C_{\mathrm{f}}U^2$ term.

2.1. Finite-volume methods

For the one-dimensional shallow-water flow, write $\mathbf{W}(x,t)=(h,hU)^{\mathrm{T}}$ as the vector of conservative flow variables, $\mathbf{F}(\mathbf{W})=(hU,hU^2+\frac{1}{2}Gh^2)^{\mathrm{T}}$ as the corresponding flux vector function, and $\mathbf{S}(\mathbf{W})=(0,-GhB'(x))^{\mathrm{T}}$ as the vector of the source terms, where the friction force will not be included in this section. Shallow-water equations (1) in the form of hyperbolic conservation

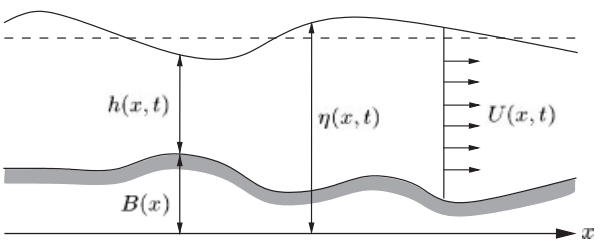

Figure 1. One-dimensional shallow-water flow in a river channel with bed topography. $h(x,t)$ is the water height above the river bottom; $U(x,t)$ is the water velocity averaged across the water height in the x-direction; $B(x)$ is the bottom elevation along the river channel; and the water top surface level, $\eta(x,t)$, is $h(x,t)+B(x)$.

equations can be written as

$$\frac{\partial \mathbf{W}}{\partial t} + \frac{\partial \mathbf{F}}{\partial x} = \mathbf{S} \tag{2}$$

Consider rectangular grids for the space discretization, with Δx the uniform mesh spacing. Let $x_i = i\Delta x$ $(i = 1, 2, \ldots, N)$ be the cell centre of cell i. We choose $x_{i+1/2} = (i + 1/2)\Delta x$ as the location of the cell interface between cells i and $i + 1$. With a finite volume method we view each discrete value $\mathbf{W}$ as a cell average over a grid cell. Introduce $\mathbf{W}_i = (h_i, hU_i)^{\mathrm{T}}$ and $\mathbf{S}_i = (0, -Gh_iB_i')^{\mathrm{T}}$ as the mean or cell averaged value of the conservative variables, $\mathbf{W}$, and the source terms, $\mathbf{S}$, in cell i, respectively. The finite-volume formulation for one-dimensional shallow-water equations is

$$\mathbf{W}_i^{n+1} = \mathbf{W}_i^n + \frac{1}{\Delta x}\int_{t^n}^{t^{n+1}} [\mathbf{F}_{i-1/2}(t) - \mathbf{F}_{i+1/2}(t)]\,\mathrm{d}t + \int_{t^n}^{t^{n+1}} \mathbf{S}_i\,\mathrm{d}t \tag{3}$$

The above equation is the shallow-water equations (1) in an integral form and equivalent to them. Physically, the source terms in (3) describe the effect of the gravitational force acting on a fluid element moving from one place to another within the same cell due to the varying river bottom. If a fluid element passes through the cell interface, the contribution of the gravitational force effect is included in the cell interface fluxes. Both the uneven river bottom and gravitational force will take effect on any fluid element moving within the same cell or passing through the cell interface in a numerical time step given by $\Delta t = t^{n+1} - t^n$. Therefore, the influence of the source terms, e.g. the fluid acceleration due to the varying river topography when a fluid is passing through the boundary of a cell, should be included in the flux function evaluated at the cell interface as well. The treatment for the integration of the source terms is discretized in the following form:

$$\int_{t^n}^{t^{n+1}} -Gh_iB_i'\,\mathrm{d}t = -G\left[\frac{h_i^n + h_i^{n+1}}{2}\right]B_i'\,\Delta t \tag{4}$$

where $\Delta t = t^{n+1} - t^n$ is the numerical time step determined by the CFL condition. The numerical flux function at a cell interface is given in the next section, where the gravitational effect due to the topography of the river is explicitly included in the flux evaluation. For most Godunov-type methods, only the homogeneous shallow-water equations are solved in the flux evaluation.

2.2. *Using the BGK kinetic model for flux evaluation*

In order to obtain an approximate solution for shallow-water equations, kinetic equation with approximate Boltzmann collision model is useful. Consider the Boltzmann equation in a one-space dimension

$$\frac{\partial f}{\partial t} + u\frac{\partial f}{\partial x} + \frac{\partial \Phi}{\partial x}\frac{\partial f}{\partial u} = Q(f, f) \tag{5}$$

where $f = f(x, t, u)$ is the real particle distribution function, which is a function of space, $x \in R$, time, $t \geqslant 0$, and particle velocity, $u \in R$; Φ_x is the gravitational force term acting on the particle due to the varying river bottom with shape $B(x)$, i.e. $\Phi_x = -GB'(x)$; and $Q(f, f)$

is the molecular collision term. The collision term is a complicated integral function that accounts for changes in f due to binary molecular collisions.

In the BGK kinetic model [2], the molecular collision integral is replaced by a relaxation term of the form

$$Q(f,f) = -\frac{1}{\tau}(f-g) \tag{6}$$

and the BGK equation with the inclusion of the gravitational force term is

$$\frac{\partial f}{\partial t} + u\frac{\partial f}{\partial x} + \frac{\partial \Phi}{\partial x}\frac{\partial f}{\partial u} = \frac{g-f}{\tau} \tag{7}$$

where $g = g(x,t,u)$ is the local equilibrium particle distribution function in which the real distribution function, f, approaches at the rate $1/\tau$, and thus τ is an average time between collisions. The collision time, τ, generally depends on the particle velocity, u, but we shall consider it as a local constant in our context. The local equilibrium state, g, is a Maxwellian distribution that maximizes the entropy for the system and takes the form

$$g = h\left(\frac{\lambda}{\pi}\right)^{1/2} \mathrm{e}^{-\lambda(u-U)^2} \tag{8}$$

where $h(x,t)$ is the water height and $U(x,t)$ is the water velocity. In order to recover the shallow-water equations, λ has to be defined as

$$\lambda = \frac{1}{Gh} \tag{9}$$

The BGK kinetic model is based on the assumption that the main effect of molecular collisions is to force the gas distribution function, f, to relax to a state of local equilibrium, g, and therefore f and g have to satisfy the conservation constraint

$$\int_{-\infty}^{+\infty} (g-f)\begin{bmatrix}1\\ u\end{bmatrix} \mathrm{d}u = \mathbf{0} \quad \forall x,t \tag{10}$$

such that f and g have the same mass and momentum. The connection between the macroscopic flow variables, $\mathbf{W}$, and the microscopic distribution function, f, in the equilibrium state with $f = g$ can be obtained by taking moments, $(1,u)^{\mathrm{T}}$, and integrating over the whole velocity space

$$\int_{-\infty}^{+\infty} f\begin{bmatrix}1\\ u\end{bmatrix} \mathrm{d}u = \int_{-\infty}^{+\infty} g\begin{bmatrix}1\\ u\end{bmatrix} \mathrm{d}u = \mathbf{W} = \begin{bmatrix}h\\ hU\end{bmatrix} \tag{11}$$

With the moment relation described in (11), the fluxes for the corresponding macroscopic variables are

$$\int_{-\infty}^{+\infty} fu\begin{bmatrix}1\\ u\end{bmatrix} \mathrm{d}u = \mathbf{F}(\mathbf{W}) = \begin{bmatrix}hU\\ hU^2 + \frac{1}{2}Gh^2\end{bmatrix} \tag{12}$$

For a local equilibrium state with $f = g$, the one-dimensional shallow-water equations with bottom topography can be obtained by taking the moments of the BGK equation (7). This yields

$$\int_{-\infty}^{+\infty} (g_t + ug_x + \Phi_x g_u) \begin{bmatrix} 1 \\ u \end{bmatrix} \mathrm{d}u = \mathbf{0} \tag{13}$$

and thus we obtain the corresponding one-dimensional shallow-water equations (2)

$$\frac{\partial}{\partial t} \begin{bmatrix} h \\ hU \end{bmatrix} + \frac{\partial}{\partial x} \begin{bmatrix} hU \\ hU^2 + \frac{1}{2} Gh^2 \end{bmatrix} = \begin{bmatrix} 0 \\ -GhB'(x) \end{bmatrix}$$

To obtain the general solution for the particle distribution function, f, in the BGK model, we follow the particle along the trajectory $\mathrm{d}x/\mathrm{d}t = u$ with the particle velocity $\mathrm{d}u/\mathrm{d}t = \Phi_x$, and the BGK equation (7) becomes

$$\frac{\mathrm{d}f}{\mathrm{d}t} + \frac{f}{\tau} = \frac{g}{\tau} \quad \text{along} \quad \frac{\mathrm{d}x}{\mathrm{d}t} = u \quad \text{and} \quad \frac{\mathrm{d}u}{\mathrm{d}t} = \Phi_x \tag{14}$$

which is a first-order linear ordinary differential equation (ODE). Replacing the variable time, t, by a primed variable, t', multiplying the integrating factor $\exp(t'/\tau)$ on both sides and integrating against $\mathrm{d}t'$ from $t' = 0$ to $t' = t$, we have

$$\mathrm{e}^{t'/\tau} f|_0^t = \frac{1}{\tau} \int_0^t g(x', t', u') \mathrm{e}^{t'/\tau} \, \mathrm{d}t' \quad \text{along} \quad \begin{cases} x = x' + u'(t - t') + \frac{1}{2} \Phi_x (t - t')^2 \\ u = u' + \Phi_x (t - t') \end{cases}$$

The integral solution of the BGK equation (7) is thus given by

$$f(x, t, u) = \frac{1}{\tau} \int_0^t g(x', t', u') \mathrm{e}^{-(t - t')/\tau} \, \mathrm{d}t' + \mathrm{e}^{-t/\tau} f_0(x_0, 0, u_0) \tag{15}$$

and holds along the particle trajectory, $x = x' + u'(t - t') + \frac{1}{2}\Phi_x (t - t')^2$, and the particle velocity change, $u = u' + \Phi_x (t - t')$, due to the effect of gravitational force. There are two unknowns to be specified in the integral solution (15). One is the initial non-equilibrium particle distribution function, f_0, around position x_0 and with particle velocity u_0 at time $t = 0$, and the other is the equilibrium state, g, in space locally around the cell interface, $x = x_{i+1/2}$, and in time locally around $t = 0$ (see Figure 2). Under the effect of gravitational force, the particle velocity will change according to $u = u' + \Phi_x (t - t')$. Suppose that a particle is moving from x' to x in a short time interval, $t - t'$, and the particle velocity will be changed from u' to u accordingly because of the gravitational acceleration of the particle. Owing to this particle velocity change, a modification to the particle velocity, u', in terms of u is needed

$$\begin{bmatrix} x' \\ t' \\ u' \end{bmatrix} \longrightarrow \begin{bmatrix} x \\ t \\ u \end{bmatrix} : \quad u = u' + \Phi_x (t - t') \quad \Rightarrow \quad u' = u - \Phi_x (t - t')$$

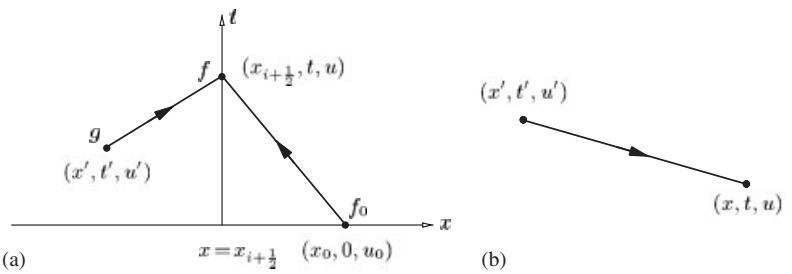

Figure 2. (a) Particle trajectory and particle velocity change; and (b) moving of a fluid particle.

The BGK scheme for shallow-water equations is based on Equation (15) for the solution of f, and the flux function, $\int u(1,u)^{\mathrm{T}} f \, \mathrm{d}u$, is based on this solution. The detailed description is given in Reference [3]. The following covers the main steps. First, the discretization of the source term, Φ_x, around $x = x_{i+1/2}$ (i.e. $x_{i-1} \leqslant x \leqslant x_i$) is written as

$$\begin{aligned}\Phi_x &= \begin{cases} -GB_i', & x < x_{i+1/2} \\ -GB_{i+1}', & x \geqslant x_{i+1/2} \end{cases} \\ &= -G[B_i'(1 - H[x - x_{i+1/2}]) + B_{i+1}' H[x - x_{i+1/2}]] \end{aligned} \tag{16}$$

where B_i' and B_{i+1}' are the constant slopes in cell i and $i+1$, respectively, and H is the Heaviside function defined by

$$H[x] = \begin{cases} 0, & x < 0 \\ 1, & x \geqslant 0 \end{cases} \tag{17}$$

The initial non-equilibrium state, f_0, is based on the Taylor expansion of a Maxwellian around each cell interface, $x_{i+1/2}$. The distribution function, f_0, at time $t = 0$ is assumed to be

$$\begin{aligned} f_0(x,0,u) &= \begin{cases} g^{\mathrm{l}}[1 + a^{\mathrm{l}}(x - x_{i+1/2})] & x < x_{i+1/2} \\ g^{\mathrm{r}}[1 + a^{\mathrm{r}}(x - x_{i+1/2})] & x \geqslant x_{i+1/2} \end{cases} \\ &= g^{\mathrm{l}}[1 + a^{\mathrm{l}}(x - x_{i+1/2})](1 - H[x - x_{i+1/2}]) + g^{\mathrm{r}}[1 + a^{\mathrm{r}}(x - x_{i+1/2})] H[x - x_{i+1/2}] \end{aligned} \tag{18}$$

where $g^{\mathrm{l}} = g^{\mathrm{l}}(t,u)$ and $g^{\mathrm{r}} = g^{\mathrm{r}}(t,u)$ are the Maxwellian distribution functions at the left and right of the cell interface, $x = x_{i+1/2}$, and a^{l} and a^{r} are the spatial derivatives of g separately, such as $(\partial g/\partial x)/g$. The Maxwellians as well as their slopes can be obtained from the reconstructed initial data of the macroscopic variables, h and hU. The equilibrium state, g, is assumed to be continuous at each cell interface, $x_{i+1/2}$, but with different slopes on the left-

and right-hand sides

$$g(x,t,u)=\begin{cases} g_0[1+\bar{a}^{\mathrm{l}}(x-x_{i+1/2})+\bar{A}t], & x<x_{i+1/2} \\ g_0[1+\bar{a}^{\mathrm{r}}(x-x_{i+1/2})+\bar{A}t], & x>x_{i+1/2} \end{cases}$$

$$=g_0[1+\bar{a}^{\mathrm{l}}(x-x_{i+1/2})(1-H[x-x_{i+1/2}])+\bar{a}^{\mathrm{r}}(x-x_{i+1/2})H[x-x_{i+1/2}]+\bar{A}t] \qquad (19)$$

where $g_0=g_0(t,u)$ is the local equilibrium state located at $(x,t)=(x_{i+1/2},0)$. Similarly, $\bar{a}$ and A are spatial and temporal derivatives of g. By substituting Equations (18) and (19) into (15), an explicit formulation of the particle distribution function at a cell interface can be obtained, from which the numerical fluxes in Equation (3) can be evaluated.

A well-balanced scheme for shallow water equations should be able to keep the exact solution of $B+h=$ constant and $U=0$. This condition is equivalent to requiring the numerical flux function at a cell interface to have only the pressure term $Gh^2/2$ in the momentum flux and zero mass flux. Even with a linear initial water height distribution, such as $\partial h/\partial x\neq 0$ and $U=0$ around a cell interface, due to the explicit inclusion of the gravitational force term in the gas distribution function, the time-accurate mass and momentum convective transport due to $\partial h/\partial x$ are exactly cancelled by the gravitational force effect, i.e. from the terms related to $G\partial B/\partial x$ in the gas distribution function. The constant parameters α in Equation (2.21) of Reference [3] are obtained by this well-balanced condition. The trapezoidal rule for the source term update in time inside each cell (4) is not necessary and it can be changed to other form, because the flux function at the cell interface in the gas-kinetic BGK scheme guarantees $h_i^{n+1}=h_i^n$ in this case. For the flow down an inclined channel, in order to have a steady state solution, i.e. $U\neq 0$ and $\partial h/\partial x=\partial U/\partial x=0$, the gravitational force and the friction force must be equal and balanced in both the flux evaluation at the cell interface and the source term update inside each cell. This is equivalent to having no source term in the original governing equations under this condition, and the cancellation of the gravitational force and the bottom friction automatically removes the source term effect in the time evolution of the gas distribution function at a cell interface in the current scheme.

The detailed formulation and extensive numerical test cases for 1D and 2D shallow-water flows can be found in References [3, 10]. The current study is about the numerical solution for the inviscid shallow-water equations. If viscous shallow-water equations need to be solved, the initial condition in Equation (18) has to include the non-equilibrium state based on the Chapmann–Enskog expansion as well [11].

3. ROLL-WAVES IN INCLINED OPEN CHANNELS

In this section, the scheme presented in the last section will be used to study the problem of roll-waves down an inclined open channel, in which the balance between the slope and the friction of the river bottom are important. In the computation, the units of length and time quantity are meters (m) and seconds (s), respectively, and the unit of speed is meters per second ($\mathrm{m\,s^{-1}}$). Unless otherwise specified, the gravitational constant takes the value $G=9.8\,\mathrm{m\,s^{-2}}$. The Froude number, F, is a dimensionless parameter defined by the ratio of

the mean water velocity to the propagating speed of small amplitude disturbances,

$$F = \frac{U}{\sqrt{Gh}} \tag{20}$$

which can also be viewed as the ratio of inertial to gravitational forces in an open channel flow. The Froude number classifies the regime of the flow:

- if $F < 1$, the flow is subcritical (tranquil flow);
- if $F > 1$, the flow is supercritical (shooting flow);
- if $F = 1$, the flow is critical (also called transcritical).

Consider a uniform flow down an inclined open river channel with bed friction. If the Froude number of the undisturbed uniform flow exceeds a certain critical value, the water surface of the flow would become unstable. In this case, when a small perturbation is imposed on the steady uniform state, the flow eventually evolves into a series of breaking waves or bores separating two sections of gradually varying flow, in a staircase pattern. This discontinuous periodic pattern is termed 'roll-waves' and was first studied by Dressler in 1949 [5]. The roll-waves progress downstream at a constant speed, with a continuous transition from subcritical to supercritical flow and transit back to subcritical flow through a hydraulic jump (shock) in a uniformly moving frame, as sketched in Figure 3. The organization in this problem mainly follows the paper by Brook–Falle–Pedley [4]. Some variables and parameter values in that publication are not described very clearly and may lead the reader to have uncertainties in following the numerical procedure. In our study, the parameter values are justified again, and the details are described as clearly as possible.

3.1. Linearized theory and stability

This physical problem is described by the shallow-water equations with source terms modelling the balance between the slope and the friction of the river bottom,

$$\begin{gathered} \frac{\partial h}{\partial t} + \frac{\partial}{\partial x}(hU) = 0 \\ \frac{\partial}{\partial t}(hU) + \frac{\partial}{\partial x}\left(hU^2 + \frac{1}{2}Gh^2\right) = GhS - C_{\mathrm{f}}U^2 \end{gathered} \tag{21}$$

where t denotes time, x is the distance along the channel, $h(x,t)$ is the water height above the river bottom, $U(x,t)$ is the mean water velocity across the water height in the x-direction,

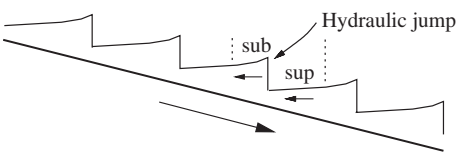

Figure 3. Sketch of roll-waves down an inclined open channel.

G is the acceleration due to gravity, and S and C_f are the slope and the friction coefficient of the river bottom, respectively.

The linearized theory establishes the stability criterion by imposing a small perturbation on a steady uniform state [4, 9]. The uniform steady solutions, $h = h_0$ and $U = U_0$, to Equations (21) are given by the balance between the gravitational and frictional forces, so that

$$h_0 U_0 = Q_0 \tag{22}$$

$$G h_0 S = C_f U_0^2 \tag{23}$$

where Q_0 is the undisturbed steady flow rate. From Equation (23) and by the definition of the Froude number, the slope of the bottom, S, is related to the friction coefficient, C_f, through

$$S = F_0^2 C_f \tag{24}$$

where F_0 is the undisturbed Froude number in the steady flow, given by

$$F_0 = \frac{U_0}{\sqrt{G h_0}} \tag{25}$$

By assuming S and C_f to be constants, we impose small perturbations, a' and b', to the steady solutions by substituting

$$h = h_0 + a'(x,t) \tag{26}$$

$$U = U_0 + b'(x,t) \tag{27}$$

into Equation (21) and neglecting all but the first power of a' and b'. Then, the linearized equations are given by

$$\begin{aligned} &\left(\frac{\partial}{\partial t} + U_0 \frac{\partial}{\partial x}\right) a' + h_0 \frac{\partial b'}{\partial x} = 0 \\ &\left(\frac{\partial}{\partial t} + U_0 \frac{\partial}{\partial x}\right) b' + G \frac{\partial a'}{\partial x} = GS\left(\frac{a'}{h_0} - \frac{2b'}{U_0}\right) \end{aligned} \tag{28}$$

By eliminating b', we obtain a single equation for a' and write it in the form

$$\frac{\partial a'}{\partial t} + C_0 \frac{\partial a'}{\partial x} = -\frac{U_0}{2GS}\left(\frac{\partial}{\partial t} + C_+ \frac{\partial}{\partial x}\right)\left(\frac{\partial}{\partial t} + C_- \frac{\partial}{\partial x}\right) a' \tag{29}$$

where

$$\begin{aligned} C_\pm &= U_0 \pm \sqrt{G h_0} \\ C_0 &= \frac{3U_0}{2} \end{aligned} \tag{30}$$

Therefore, the waves travel with the fastest speed, C_+, and the slowest speed, C_-. The lower order approximation

$$\frac{\partial a'}{\partial t} + C_0 \frac{\partial a'}{\partial x} \approx 0 \tag{31}$$

makes Equation (29) have positive diffusion coefficient only when $C_- < C_0 < C_+$. Equivalently, by using (30), we get the inequality

$$U_0 < 2\sqrt{Gh_0} \tag{32}$$

which is the condition for the stable steady flow. From (23), the stability condition (32) may also be expressed as

$$S < 4C_\mathrm{f} \tag{33}$$

reflecting the fact that the slope, S, of the river bed should be small compared to the friction coefficient, C_f, in order to maintain the stability of the inclined uniform flow.

3.2. Instability and the evolution of roll-waves

Condition (33) may be violated in steep channels and, under suitable conditions, roll-waves will be formed. In comparison with Equation (24), condition (33) is equivalent to the undisturbed Froude number, F_0, which has to be smaller than 2 for the stability condition to hold. In other words, perturbations to the steady solutions will grow if

$$F_0 > 2 \tag{34}$$

The amplitude growth or decaying rate of the flow down an inclined channel can be obtained from the linearized theory by assuming exponential solutions of the linearized equation (29), i.e. the small perturbation a' takes the form

$$a' \propto \mathrm{e}^{\mathrm{i}(kx-\omega t)} \tag{35}$$

where k is the 2π-wavenumber (multiple of 2π) and $\omega = \omega_R + \mathrm{i}\omega_I$, with $\mathrm{i} = \sqrt{-1}$. Substituting for a' in the linearized equation (29) gives

$$-\omega + \frac{3U_0}{2}k = -\frac{U_0}{2GS}[\mathrm{i}\omega^2 - 2U_0\mathrm{i}k\omega + U_0^2\mathrm{i}k^2 - Gh_0\mathrm{i}k^2] \tag{36}$$

and, on simplifying (36), we determine the following dispersion relation:

$$\omega^2 + \beta\omega + \gamma = 0 \tag{37}$$

where

$$\begin{aligned} \beta &= -2U_0k + \frac{2C_\mathrm{f}U_0}{h_0}\mathrm{i} \\ \gamma &= (U_0^2 - Gh_0)k^2 - \frac{3C_\mathrm{f}U_0^2}{h_0}k\mathrm{i} \end{aligned} \tag{38}$$

and thus ω is given by

$$\omega = \frac{-\beta + \sqrt{\beta^2 - 4\gamma}}{2} \tag{39}$$

From relation (35), we have

$$\ln|h - h_0| = \ln C + \omega_I t + \mathrm{i}(kx - \omega_R t) \tag{40}$$

where C is a constant. This implies that the natural logarithm of the amplitude of the water waves against time should yield a straight-line graph with slope ω_I, given by the imaginary part of ω in (39). The exponential growth rate ω_I predicted from the linear theory will be compared with that obtained from the numerical computation by giving the wavenumber, k, for the initial disturbance, the friction coefficient, C_f, the undisturbed steady flow rate, Q_0, and the undisturbed Froude number, F_0. In the computation, the initial uniform state, i.e. the water height, h_0, and velocity, U_0, are determined from (22), (23) and (25), and are given by

$$h_0 = \left(\frac{1}{G}\frac{Q_0^2}{F_0^2}\right)^{1/3} \tag{41}$$

$$U_0 = \frac{Q_0}{h_0} \tag{42}$$

In the finite-volume formulation of the BGK scheme, the bed slope term, GhS, and the bed shear stress term, $-C_\mathrm{f}U^2$, in the momentum equation of (21) will be discretized as

$$\int_0^{\Delta t} Gh_i S - C_\mathrm{f} U_i^2 \,\mathrm{d}t = Gh_i^n S\Delta t - C_\mathrm{f}(U_i^n)^2\Delta t \tag{43}$$

where Δt is the time step. The boundary conditions are taken to be periodic such that the boundary values on the left and right boundaries coincide

$$\mathbf{W}(x_\mathrm{l}) = \mathbf{W}(x_\mathrm{r}) \tag{44}$$

where x_l and x_r are the locations of the left and right ends of the computational domain in the channel.

From (35), putting $a' = h_0\varepsilon\,\mathrm{e}^{\mathrm{i}(kx-\omega t)}$ and considering its real part in (22) suggest that the initial condition for water height is a sine wave perturbation of the steady solution given by

$$h(x,0) = h_0[1 + \varepsilon\sin(kx)] \tag{45}$$

where the small parameter, ε, is an amplification factor of the initial disturbance of the water height and k is a wavenumber to be compatible with the boundary conditions. Perturbations in 0.5% of water height in the initial uniform steady flow would be used for all flow simulations, i.e. $\varepsilon = 0.005$. For the corresponding initial velocity perturbation to be compatible with the initial water height in (45), we solve the first equation of (28) for b' and consider its real part. It turns out that the corresponding initial velocity has to be

$$U(x,0) = U_0 + r_p\,\varepsilon\sin(kx + \theta_p) \tag{46}$$

where

$$\frac{\omega}{k} - U_0 = r_p\mathrm{e}^{\mathrm{i}\theta_p}, \quad \begin{cases} r_p = \left|\dfrac{\omega}{k} - U_0\right| \\ \theta_p = \arg\left(\dfrac{\omega}{k} - U_0\right) \end{cases} \tag{47}$$

where ω is given in (39) and θ_p is the phase lag between the initial water height and velocity perturbation. The solutions for water height, h, against distance, x, down the channel with

slope, S, at increasing time, t, are simulated using the BGK numerical scheme, and the solution profiles are presented in Figure 4, where the steady uniform flow is subjected to an initial disturbance with the parameter values of $\varepsilon = 0.005$, $k = 10\pi$, $C_f = 0.006$, $Q_0 = 0.001\,\mathrm{m^2\,s^{-1}}$, and $F_0 = 2.5$. The slope, S, is given by (24), i.e. $S = C_f F_0^2$. The locations of the left and right ends of the computational domain in the channel are chosen to be $x_l = 0$ and $x_r = 2$, and with 1000 grid points used in the simulation.

For the same set of parameter values (ε, k, C_f and Q_0) used in the above flow simulation, comparisons are made between the values of growth rates obtained from the linear theory and those obtained numerically by the plots of the natural logarithm of the wave amplitude, $\ln(\max|h - h_0|)$ against time, t, for different initially undisturbed Froude numbers, F_0, which are shown in Figure 5. The solid line represents the solution obtained numerically by the BGK scheme, and the dotted line represents the straight line graph of the theoretical result with a gradient of ω_I, given by the imaginary part of ω in (39) from linear analysis. For $F_0 > 2$, the amplitudes initially grow exponentially like $\exp(\omega_I t)$, as expected. However, as pointed out by Yu and Kevorkian [12], linear theory would be invalid when the non-linear terms eventually became important and came into effect as time evolved, as shown in the graph for $t \to \infty$, since we have ignored the effect of small non-linear terms in (26) and (27). Therefore, the predicted exponential growth in the amplitude is no longer valid as $t \to \infty$. The amplitude growth slows down and eventually settles down to a constant value, while the initial disturbances converge to a quasi-steady solution in the form of roll-waves that move with a constant speed without distortion. For $F_0 = 2$, a horizontal straight line graph is obtained, meaning that there is no amplitude growth, as expected, since ω_I is zero. For $F_0 < 2$, the amplitude decays since ω_I is negative. Thus, the value of the undisturbed Froude number, F_0, falling into different sides of the critical value, $F_0 = 2$, governs a totally different flow behaviour in a sloping open channel flow.

3.3. An analytical roll-wave solution

A comparison is made between the final converged roll-wave solution from the BGK scheme and that constructed analytically by Dressler [5]. The analysis of the quasi-steady solution of roll-waves comprehensively described by Dressler is summarized here.

Since roll-waves are steady in a uniformly translating frame of reference, we seek a change of variables

$$\xi = x - c_* t \tag{48}$$

where c_* is the constant progressing speed of the roll-wave flow travelling down the channel. The roll-wave solution thus takes the form

$$h(x,t) = h(\xi) \tag{49}$$

$$U(x,t) = U(\xi) \tag{50}$$

giving

$$\frac{\partial h}{\partial x} = \frac{\mathrm{d}h}{\mathrm{d}\xi}, \quad \frac{\partial h}{\partial t} = -c_* \frac{\mathrm{d}h}{\mathrm{d}\xi}$$

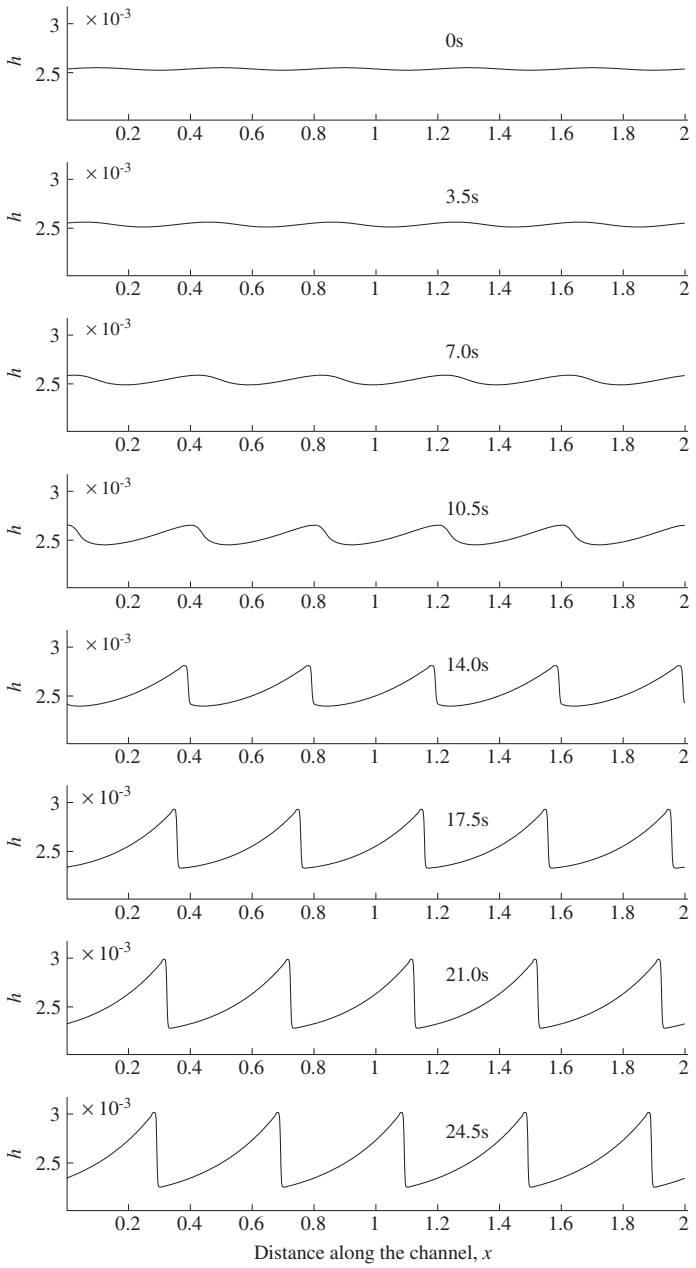

Figure 4. Evolution of roll-waves emerged out of an initially unstable uniform flow down an inclined open channel. Plots of water height, h, against distance, x, along the channel, with the slope given by $S = C_f F_0^2$, at time $t = 0$ s and the subsequent growth in time at $t = 3.5, 7.0, 10.5, 14.0, 17.5, 21.0$ and 24.5 s are shown. Solutions are for the parameter values of $\varepsilon = 0.005$, $k = 10\pi$, $C_f = 0.006$, $Q_0 = 0.001\,\mathrm{m^2\,s^{-1}}$, and $F_0 = 2.5$.

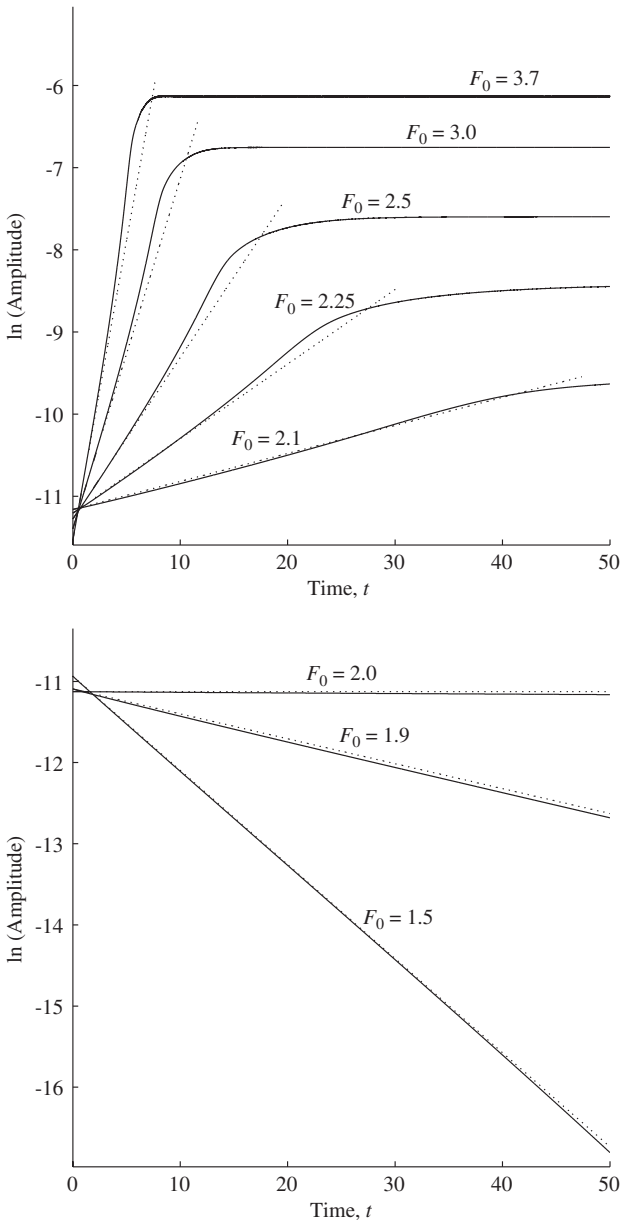

Figure 5. The natural logarithm of the amplitude, $\ln(\max|h-h_0|)$, of water waves against time t, for different initially undisturbed Froude numbers, $F_0 = 1.5, 1.9, 2.0, 2.1, 2.25, 2.5, 3.0$ and 3.7. Solid curves represent the solution obtained from the numerical BGK scheme, while dotted lines indicate the corresponding growth rates obtained from linear theory. The parameter values are $\varepsilon = 0.005$, $k = 10\pi$, $C_f = 0.006$, and $Q_0 = 0.001\,\mathrm{m^2\,s^{-1}}$.

and likewise for U. The continuity equation of (21) becomes

$$\begin{aligned} -c_* \frac{\mathrm{d}h}{\mathrm{d}\xi} + h\frac{\mathrm{d}U}{\mathrm{d}\xi} + U\frac{\mathrm{d}h}{\mathrm{d}\xi} = 0 \\ \frac{\mathrm{d}}{\mathrm{d}\xi}[h(c_* - U)] = 0 \end{aligned} \tag{51}$$

In this case h, U and c_* are related through

$$h(c_* - U) \equiv K \tag{52}$$

where K is a constant having equal value of flow rate when viewed from the uniformly translating wave frame, called the progressive flow rate.

It has been shown by Dressler that in the smooth section connecting two hydraulic jumps, there must be a smooth transition from subcritical to supercritical flow in the uniformly translating frame of reference of the waves and such that there exists a point, ξ_c, where the flow is critical (see Figure 6). We shall use the subscript c to refer to quantities associated with the special solution evaluated at the critical point, ξ_c, at which the critical water height and velocity are given by

$$h_c = \frac{1}{G}\left(\frac{c_*}{1+\sqrt{S/C_f}}\right)^2 \tag{53}$$

$$U_c = \frac{c_*}{1+\sqrt{C_f/S}} \tag{54}$$

and at which the critical progressive flow rate K_c is given by

$$K_c = h_c(c_* - U_c) \tag{55}$$

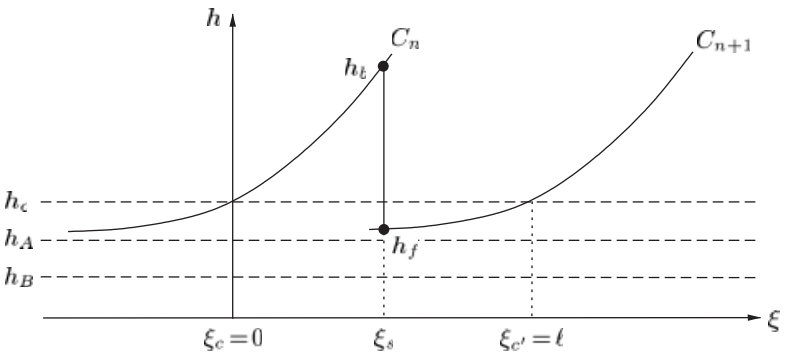

Figure 6. Two special solutions of roll-waves joined by a shock. h_A and h_B are the roots of Equation (57). h_c is the critical height through which there is a smooth transition from subcritical to supercritical flow. Curves C_n and C_{n+1} are given by Equation (56). h_b and h_f refer to maximum and minimum wave heights, respectively.

Without loss of generality, set $\xi_c = 0$. As derived in Reference [5], the function of water height, $h(\xi)$, in the continuous section through $\xi_c = 0$ is given by the inverse of

$$\xi(h) = \frac{1}{S}\left[(h - h_c) + \frac{h_A^2 + h_c h_A + h_c^2}{h_A - h_B}\ln\left(\frac{h - h_A}{h_c - h_A}\right) - \frac{h_B^2 + h_c h_B + h_c^2}{h_A - h_B}\ln\left(\frac{h - h_B}{h_c - h_B}\right)\right] \tag{56}$$

where h_A and h_B are roots of the quadratic equation in h_*

$$h_*^2 + \left(h_c - \frac{c_*^2 C_f}{GS}\right)h_* + \frac{C_f h_c^2}{S} = 0 \tag{57}$$

and we shall call the larger root h_A. Thus, we have the inequality

$$0 < h_B < h_A < h_c \tag{58}$$

The water height, $h(\xi)$, appears in (56) implicitly can be solved numerically by the iterative Newton–Raphson's method

$$h_{n+1} = h_n - \frac{f_1(h_n)}{f_1'(h_n)} \tag{59}$$

where

$$f_1(h) = h - h_c + \frac{h_A^2 + h_c h_A + h_c^2}{h_A - h_B}\ln\left(\frac{h - h_A}{h_c - h_A}\right) - \frac{h_B^2 + h_c h_B + h_c^2}{h_A - h_B}\ln\left(\frac{h - h_B}{h_c - h_B}\right) - \xi S \tag{60}$$

and

$$f_1'(h) = 1 + \frac{h_A^2 + h_c h_A + h_c^2}{h_A - h_B}\frac{1}{h - h_A} - \frac{h_B^2 + h_c h_B + h_c^2}{h_A - h_B}\frac{1}{h - h_B} \tag{61}$$

The hydraulic jump conditions are used to calculate the values of wave heights in front of and behind the jump, h_f (min) and h_b (max), i.e. $h_b > h_f > 0$, given by

$$h_f = \frac{1}{2}\left[\left(h_b^2 + \frac{8K_c^2}{Gh_b}\right)^{1/2} - h_b\right] \tag{62}$$

in which h_b and h_f are related implicitly upon using (56)

$$(h_b - h_f) + \frac{h_A^2 + h_c h_A + h_c^2}{h_A - h_B}\ln\left(\frac{h_b - h_A}{h_f - h_A}\right) - \frac{h_B^2 + h_c h_B + h_c^2}{h_A - h_B}\ln\left(\frac{h_b - h_B}{h_f - h_B}\right) - \ell S = 0 \tag{63}$$

where ℓ is the distance between two consecutive bores in the quasi-steady solution and can be determined from the wavenumber, k of the original small disturbance, and hence the positions of the jump relative to ξ_c can be obtained from (56). Again, the water height behind the jump, h_b, which appears in (63), implicitly can be solved numerically by

$$(h_b)_{n+1} = (h_b)_n - \frac{f_2((h_b)_n)}{f_2'((h_b)_n)} \tag{64}$$

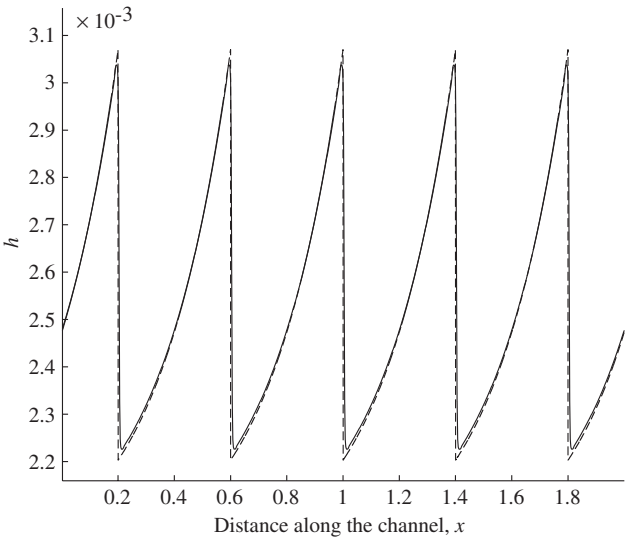

Figure 7. Comparison between the converged roll-wave solution obtained numerically from the BGK scheme and that analytically constructed by Dressler [5]. The solid curve shows the numerical solution and the broken curve represents the theoretical solution.

where

$$f_2(h_\mathrm{b}) = h_\mathrm{b} - h_\mathrm{f} + \frac{h_A^2 + h_\mathrm{c}h_A + h_\mathrm{c}^2}{h_A - h_B}\ln\left(\frac{h_\mathrm{b} - h_A}{h_\mathrm{f} - h_A}\right) - \frac{h_B^2 + h_\mathrm{c}h_B + h_\mathrm{c}^2}{h_A - h_B}\ln\left(\frac{h_\mathrm{b} - h_B}{h_\mathrm{f} - h_B}\right) - \ell S \tag{65}$$

and

$$f_2'(h_\mathrm{b}) = 1 - h_\mathrm{f}' + \frac{h_A^2 + h_\mathrm{c}h_A + h_\mathrm{c}^2}{h_A - h_B}\left[\frac{1}{h_\mathrm{b} - h_A} - \frac{h_\mathrm{f}'}{h_\mathrm{f} - h_A}\right] - \frac{h_B^2 + h_\mathrm{c}h_B + h_\mathrm{c}^2}{h_A - h_B}\left[\frac{1}{h_\mathrm{b} - h_B} - \frac{h_\mathrm{f}'}{h_\mathrm{f} - h_B}\right] \tag{66}$$

with

$$h_\mathrm{f}' = \frac{1}{2}\left[\left(h_\mathrm{b} - \frac{4K_\mathrm{c}^2}{Gh_\mathrm{b}^2}\right)\left(h_\mathrm{b}^2 + \frac{8K_\mathrm{c}^2}{Gh_\mathrm{b}}\right)^{-1/2} - 1\right] \tag{67}$$

Relevant parameter values of the quasi-steady solution shown in Figure 4 are, respectively, substituted into Equations (53)–(55) to obtain the critical water height, h_c, velocity, U_c, and the critical progressive flow rate, K_c, for the construction of the theoretical roll-wave

solution, and a comparison between the numerical and analytical solutions is made. It should be emphasized that the constant progressing speed, c_*, of a roll-wave is obtained from our numerical result, and the value measured is found to be $c_* = 0.56\,\mathrm{m\,s^{-1}}$. The result of the comparison is shown in Figure 7, where the solid line represents the solution obtained from the BGK numerical calculation and the broken curve represents the analytical solution. It can be seen that very good agreement is achieved.

4. RUN-UP OF SOLITARY WAVES

4.1. Solitary waves and the KdV equation

The solitary wave is a single symmetric hump above an undisturbed depth of water propagating at uniform speed without change of shape [1] (see Figure 8). 'Solitary waves' were named by John Scott Russell, who was the first to observe the phenomenon of a large bulge of water slowly travelling along a channel of water in 1834. He subsequently conducted a number of detailed laboratory experiments to investigate the nature of the phenomena. He found that the waves are long, shallow-water waves of permanent form progressing on the surface of the water, and the speed of the propagation, c, of a solitary wave in a channel of uniform depth, h_0, is given by

$$c = \sqrt{G(h_0 + H)} \tag{68}$$

where H is the amplitude of the wave and G is the gravitational acceleration. Later at the end of the nineteenth century, physicists Korteweg and deVries proposed a non-linear evolution equation to model the height of long surface gravity waves propagating in a shallow channel of water [13]

$$\frac{\partial \mu}{\partial t} + c_0 \frac{\partial \mu}{\partial x} + \frac{3c_0}{2h_0}\mu\frac{\partial \mu}{\partial x} + \frac{c_0 h_0^2}{6}\frac{\partial^3 \mu}{\partial x^3} = 0 \tag{69}$$

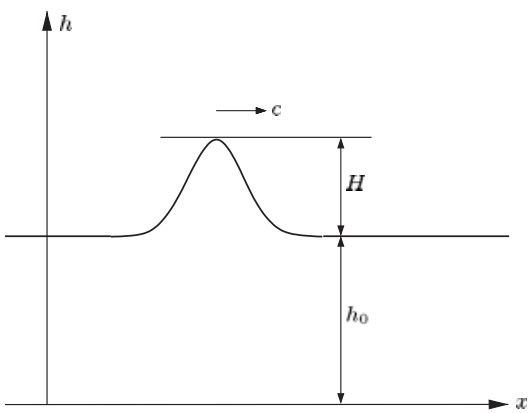

Figure 8. Sketch of a solitary wave. It is a single symmetric hump of height H above the undisturbed depth of water, h_0, propagating at uniform speed, c, without change of shape.

where $c_0 = \sqrt{Gh_0}$ and the water height, h is $h_0 + \mu$. Equation (69) is a third-order non-linear partial differential equation known as the Korteweg–deVries (KdV) equation. In particular, if we assume a solution in the form of a travelling wave, $\mu(x,t) = f(x - ct)$, then (69) can be integrated by imposing the boundary conditions at large distances that $\mu(x,t)$ tends to 0 sufficiently fast as $x \to \pm\infty$.

4.2. *Run-up of solitary waves on sloping beaches*

The problem of determining the run-up of solitary waves climbing on planar sloping beaches arises in the study of the effects of tsunamis in coastal regions. Tsunamis are sea waves of extremely long wavelengths and long periods, generated in a body of water by an impulsive disturbance such as underwater earthquakes, landslides or volcanic activity, that displace the water and travel across the ocean. It is because of their extremely long wavelengths that tsunamis are characterized as shallow-water waves (long waves). A wave behaves as a shallow-water wave when the ratio between the water height and its wavelength is very small. In shallow-water waves, the speed of propagation of a small amplitude wave is equal to the square root of the product of the gravitational acceleration and the water height. The rate at which a wave loses its energy is inversely related to its wavelength. Since a tsunami has a very large wavelength, it will lose little energy as it propagates. Hence, in very deep water, a tsunami will travel at high speeds and great distances with limited energy loss. As a tsunami leaves the deep water of the open sea and propagates into the more shallow-water near the coast, its height grows significantly, with the change of total energy remaining constant. When a tsunami finally reaches near the shoreline, it may appear as a rapidly rising or falling tide, or a series of breaking waves. The maximum vertical height that tsunami reaches onshore above the sea level is called a run-up height. In extreme cases, the water level rises to flood the coastal area, covering large expanses of land with water and debris, causing significant destruction. Since most of the damage associated with tsunamis is related to their run-up at the shoreline, understanding and being able to predict the run-up associated with such long incident breaking waves is an important aspect of understanding seismic activity. It is believed that solitary waves can model well some important aspects of the coastal effects of tsunami.

We consider a bottom topography consisting of a uniform sloping beach of angle ϕ ($0 < \phi < \pi/2$) or slope $\tan\phi$, connected to an open ocean of constant depth, h_0, as depicted in Figure 9. The origin of the co-ordinate system is at the initial position of the shoreline. The topography is described by

$$B(x) = \begin{cases} -h_0 x \tan\phi & \text{when } x \geqslant \cot\phi \\ -h_0 & \text{when } x < \cot\phi \end{cases} \tag{70}$$

Consider a propagation problem described by shallow-water equations with bottom topography

$$\begin{gathered} \frac{\partial h}{\partial t} + \frac{\partial}{\partial x}(hU) = 0 \\ \frac{\partial}{\partial t}(hU) + \frac{\partial}{\partial x}\left(hU^2 + \frac{1}{2}Gh^2\right) = -GhB'(x) \end{gathered} \tag{71}$$

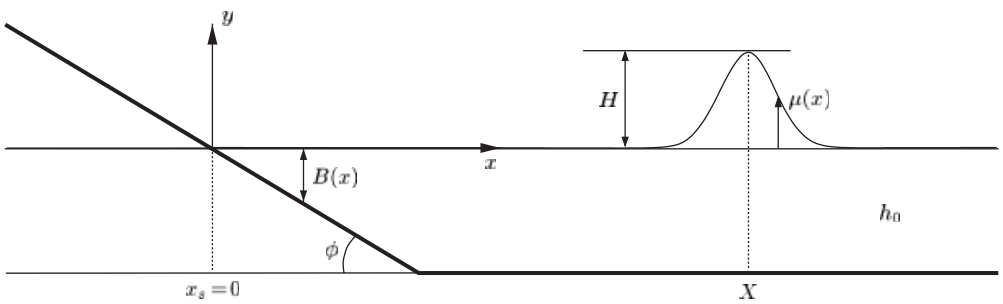

Figure 9. A solitary wave climbing up a sloping beach.

where t denotes time, x is the distance along the channel, $h(x,t)$ is the water height above the ocean bottom, $U(x,t)$ is the water velocity averaged across the water height in the x-direction, $B(x)$ is the topography given in (70), and G is the acceleration due to gravity.

Difficulties arise in the treatment of the shoreline position when applying (71) to the run-up of a solitary wave [6]. This is because the shoreline moves as the water washes up and down the sloping beach during the run-up process. Therefore, a special treatment is included in the numerical model to define the shoreline. In the scheme, an artificial or bed-wetting parameter, h_{dry}, for a dry bed is numerically defined to treat the moving shoreline. When the water height in the cell is less than h_{dry}, the water height, h, will be reset to h_{dry}, the momentum, hU, will be set to zero, and the cell is considered 'dry', i.e. no water and with zero momentum. Otherwise, the cell is occupied by water and is interpreted as 'wet'. The shoreline is defined as the line of separation between the 'dry' and the 'wet' cells. In the program code, the value of h_{dry} is taken to be 10^{-4}.

The offshore boundary condition is taken to be transmissive such that the components of the conservative variable at the offshore boundary do not change in the direction normal to the boundary, i.e.

$$\left.\frac{\partial \mathbf{W}}{\partial x}\right|_{x_r} = \mathbf{0} \tag{72}$$

where x_r is the location of the right end (offshore) of the computational domain. In the onshore boundary, the 'dry' bed is imposed as the boundary condition, where the water height is given by h_{dry} and the momentum is zero, i.e.

$$h(x_l) = h_{\text{dry}} \tag{73}$$

$$hU(x_l) = 0 \tag{74}$$

where x_l is the location of the left end (onshore) of the computational domain. In the discrete case, the boundary conditions are given by setting values of height, h, and momentum, hU, at the boundary equal to their neighbouring values inside the domain, i.e.

$$h_{-1} = h_{\text{dry}} \quad h_0 = h_{\text{dry}} \quad h_{N+1} = h_N \quad h_{N+2} = h_N$$

$$hU_{-1} = 0 \quad hU_0 = 0 \quad hU_{N+1} = hU_N \quad hU_{N+2} = hU_N$$

where the flow variables with subscripts 1 and N indicate that the flow variables are in the computational cells, while with $-1, 0, N+1$ and $N+2$ are in the ghost cells added to the computational domain.

The initial water height and velocity are, respectively, given by

$$h(x,0) = \mu(x) - B(x) \tag{75}$$

and

$$U(x,0) = \frac{c\mu}{1+\mu} \tag{76}$$

In the above expressions, $B(x)$ is the bottom topography given in (70), $\mu = \mu(x)$ is the initial solitary wave shape given by

$$\mu(x) = H \operatorname{sech}^2\left[\sqrt{\frac{3H}{4h_0^3}}\,(x - X)\right] \tag{77}$$

and c is the wave celerity given by

$$c = \sqrt{G(h_0 + H)} \tag{78}$$

where h_0 is the undisturbed depth of the water and H is the initial amplitude of the solitary wave with the initial wave crest centred at the position $x = X$, as shown in Figure 9.

The profiles of the water surface, η, against distance, x, of an incident solitary wave initially located at position $X = 14.0$ with an initial wave amplitude, $H = 0.3$, and undisturbed water depth, $h_0 = 1$, climbing up a sloping beach with slope 1:19.85 at increasing time, t, are simulated using the BGK numerical scheme. In the numerical computation, the locations of the left and right ends of the computational domain are chosen to be $x_\mathrm{l} = -20$ and $x_\mathrm{r} = 25$, and grids of 1000 cells are used. The computation breaks down after $t \simeq 19$ s due to the run-down process. Comparisons of the water surface elevation, η, against distance, x, at different times, t, are made between the numerical and experimental results, which are given in Figure 10. The figure shows both the run-up and run-down processes. The solid line is the result of the numerical simulation from the BGK scheme, and the dots are the experimental data [6]. The experiments were performed in the wave tank located at the California Institute of Technology by Synolakis in 1986.

Figure 10(a) shows the initial wave profile. The numerical data matches the experimental data initially. As time increases and the wave propagates, the front face becomes steeper than the rear face and the wave shape becomes asymmetrical (see Figure 10(b) and (c)). The numerical results clearly show this trend and are reasonably well confirmed by the experimental data. The front face becomes steeper and steeper and ultimately is vertical. The position at which this occurs is defined as the breaking point in the numerical model. The shock-like front face of the breaking wave can also be seen in Figure 10(b) and (c). There appears to be a difference in the location of the front face of the breaking wave between the numerical data and experimental data as seen in Figure 10(c). This difference may be caused by the modelling error in the shallow-water equations in the breaking wave region.

As the breaking wave propagates up the slope, it collapses near the initial shoreline position and the wave height decreases dramatically, but the shape changes slowly in the region away from the front tip of the wave. The agreement between the numerical and experimental

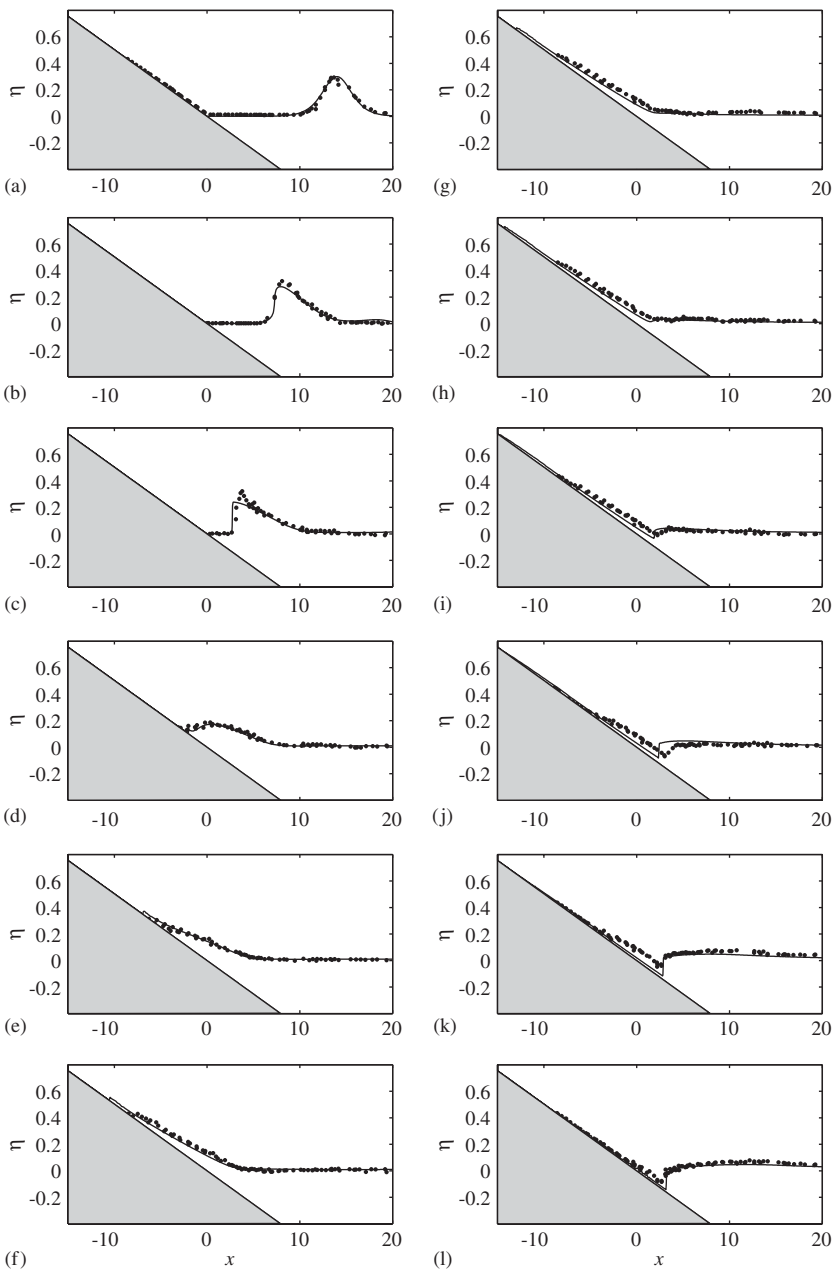

Figure 10. Run-up of a solitary wave with $H/h_0 = 0.3$ on 1:19.85 slope. Water surface profiles, η, are shown as functions of distance, x, from the initial shoreline at different times, t. Solid lines are solutions of the numerical simulation from the BGK scheme, and dots are the experimental data in Reference [6]. (a) $t = 0$s, (b) $t = 1.60$s, (c) $t = 3.19$s, (d) $t = 4.79$s, (e) $t = 6.39$s, (f) $t = 7.99$s, (g) $t = 9.58$s, (h) $t = 11.18$s, (i) $t = 12.78$s, (j) $t = 14.38$s, (k) $t = 15.97$s, (l) $t = 17.57$s.

results shown in Figure 10(d)–(f) is very good. There are very slight differences between the numerical and experimental data near the run-up tip as seen in Figure 10(g)–(i). The difference in the region after the wave breaks and in the vicinity of the run-up tip may be due to the effect of bottom friction, which is not included in the numerical model.

The wave run-down process begins after the wave reaches its maximum run-up position. The hydraulic jump is developed near the initial shoreline after a wave has completely broken in the final stage of its run-up, as seen in Figure 10(j)–(l). Both the position of the jump and the height difference across the jump are predicted quite well by the numerical method, except in Figure 10(j). Again, this exception may be due to the governing equations used here, where the vertical direction movement of the fluid is ignored, which may have a significant impact on the wave breaking. The height difference near the initial shoreline may be again due to the effect of bottom friction being ignored.

5. CONCLUSION

In this paper, the gas-kinetic BGK scheme is introduced and used in the study of roll-wave and solitary wave propagation. Firstly, shallow-water equations are recovered mathematically by a gas-kinetic BGK model, where the particle acceleration in the Boltzmann equation due to the gravitational force corresponds precisely to the non-homogeneous term in the macroscopic equations from the bottom topography. The numerical flux explicitly follows the particle motion across the cell interface with the inclusion of particle acceleration and deceleration. For roll-waves in an inclined open channel, the detailed formulation for the linear stability and Dressler's roll-wave solution are presented, which have excellent agreement with the numerical computations. For run-up solitary waves, the simulation results compare well with experimental measurements, such as the maximum run-up and the wave profiles, even though the detailed wave breaking process cannot be described by the current numerical model.

ACKNOWLEDGEMENTS

The authors thank reviewers for their constructive comments and the support from Hong Kong Research Grant Council under HKUST6116/03E, 6102/04E, and HIA04/05.EG02.

REFERENCES

1. Stoker JJ. *Water Waves*: *The Mathematical Theory with Applications*. Wiley: New York, 1958.
2. Bhatnagar PL, Gross EP, Krook M. A model for collision processes in gases. I: small amplitude processes in charged and neutral one-component systems. *Physical Review* 1954; **94**:511–525.
3. Xu K. A well-balanced gas-kinetic scheme for the shallow-water equations with source terms. *Journal of Computational Physics* 2002; **178**:533–562.
4. Brook BS, Falle SAEG, Pedley TJ. Numerical solutions for unsteady gravity-driven flows in collapsible tubes: evolution and roll-wave instability of a steady state. *Journal of Fluid Mechanics* 1999; **396**:223–256.
5. Dressler RF. Mathematical solution of the problem of roll-waves in inclined open channels. *Communications on Pure and Applied Mathematics* 1949; **2**:149–194.
6. Synolakis CE. The run-up of solitary waves. *Journal of Fluid Mechanics* 1987; **185**:523–545.
7. Bilingham J, King AC. *Wave Motion*. Cambridge University Press: Cambridge, MA, 2000.
8. Toro EF. *Shock-capturing Methods for Free-surface Shallow Flows*. Wiley: New York, 2001.
9. Whitham J. *Linear and Nonlinear Waves*. Wiley: New York, 1974.
10. Que YT. BGK kinetic scheme for the shallow-water equations. *MPhil Thesis*, The Hong Kong University of Science and Technology, 2003.

11. Xu K. A gas-kinetic BGK scheme for the Navier–Stokes equations and its connection with artificial dissipation and Godunov method. *Journal of Computational Physics* 2001; **171**:289–335.
12. Yu J, Kevorkian J. Nonlinear evolution of small disturbances into roll waves in an inclined open channel. *Journal of Fluid Mechanics* 1992; **243**:575–594.
13. Crapper GD. *Introduction to Water Waves*. Ellis Horwood: Chichester, U.K., 1984.

